THE JOURNAL OF BIOLOGICAL CHEMISTRY VOL. 283, NO. 46, pp. 31417–31428, November 14, 2008

Identification of *Mycobacterium tuberculosis* Clinical Isolates with Altered Phagocytosis by Human Macrophages Due to a Truncated Lipoarabinomannan*[S]

Received for publication, August 15, 2008, and in revised form, September 10, 2008 Published, JBC Papers in Press, September 10, 2008, DOI 10.1074/jbc.M806350200

Jordi B. Torrelles[‡], Rose Knaup[‡], Avina Kolareth[§], Tatiana Slepushkina[§], Thomas M. Kaufman[§], Peter Kang[§], Preston J. Hill[¶], Patrick J. Brennan[¶], Delphi Chatterjee[¶], John T. Belisle[¶], James M. Musser[‖], and Larry S. Schlesinger[‡1]

From the [‡]Center for Microbial Interface Biology, Division of Infectious Diseases, Departments of Internal Medicine; Molecular Virology, Immunology, and Medical Genetics; and Microbiology, Ohio State University, Columbus, Ohio 43210, the [§]Departments of Medicine, Microbiology, and Pathology, University of Iowa, Iowa City, Iowa 52240, the [¶]Mycobacteria Research Laboratories, Department of Microbiology, Immunology, and Pathology, Colorado State University, Fort Collins, Colorado 80523, and the [‖]Center for Molecular and Translational Human Infectious Diseases Research and Department of Pathology, Methodist Hospital Research Institute, Houston, Texas 77030

Phenotypically distinct clinical isolates of *Mycobacterium tuberculosis* are capable of altering the balance that exists between the pathogen and human host and ultimately the outcome of infection. This study has identified two *M. tuberculosis* strains (*i.e.* HN885 and HN1554) among a bank of clinical isolates with a striking defect in phagocytosis by primary human macrophages when compared with strain Erdman, a commonly used laboratory strain for studies of pathogenesis. Mass spectrometry in conjunction with NMR studies unequivocally confirmed that both HN885 and HN1554 contain truncated and more branched forms of mannose-capped lipoarabinomannan (ManLAM) with a marked reduction of their linear arabinan (corresponding mainly to the inner Ara*f*-α(1→5)-Ara*f* unit) and mannan (with fewer 6-Man*p* residues and more substitutions in the linear Man*p*-α(1→6)-Man*p* unit) domains. The truncation in the ManLAM molecules produced by strains HN885 and HN1554 led to a significant reduction in their surface availability. In addition, there was a marked reduction of higher order phosphatidyl-*myo*-inositol mannosides and the presence of dimycocerosates, triglycerides, and phenolic glycolipid in their cell envelope. Less exposed ManLAM and reduced higher order phosphatidyl-*myo*-inositol mannosides in strains HN885 and HN1554 resulted in their low association with the macrophage mannose receptor. Despite reduced phagocytosis, ingested bacilli replicated at a fast rate following serum opsonization. Our results provide evidence that the clinical spectrum of tuberculosis may be dictated not only by the host but also by the amounts and ratios of surface exposed mycobacterial adherence factors defined by strain genotype.

Tuberculosis causes immense morbidity and mortality worldwide (1). The causative bacterium, *Mycobacterium tuberculosis*, is phagocytosed by and grows within host macrophages. Our recent studies (2, 3) have led to the conclusion that *M. tuberculosis* is adapting to the human host by cloaking its cell envelope molecules with terminal mannosylated (*i.e.* Man-α(1→2)-Man) oligosaccharides that resemble the glycoforms of mammalian mannoproteins (4). These molecules include the abundant mannose-capped lipoarabinomannan (ManLAM),[2] lipomannan (LM), and phosphatidyl-*myo*-inositol mannosides (PIMs), which play a central role in *M. tuberculosis* immunopathogenesis (5). ManLAM and higher order PIMs (*i.e.* PIM_5 and PIM_6) have exposed Man-α(1→2)-Man nonreducing termini that engage the mannose receptor (MR) on human macrophages during phagocytosis (3, 6, 7) and dictate the intracellular fate of *M. tuberculosis* by regulating formation of the unique vesicular compartment in which *M. tuberculosis* survives within the human host (2, 3).

To date, studies of *M. tuberculosis* phagocytosis have focused largely on use of the common laboratory virulent strains Erdman and $H_{37}R_v$ and the attenuated strain $H_{37}R_a$. Recently, banks of clinical isolates have been characterized in an attempt to link epidemiology and genetic analyses in order to better understand the pathogenesis of the tuberculosis (8–11). These population studies classified *M. tuberculosis* into three distinct genetic groups, designated principal genetic group 1, 2, and 3 (PGG-1, -2, and -3), based on allelic variation in genes encoding gyrase and catalase-peroxidase (8), two genes involved in antibiotic resistance (12, 13), and the pattern of the insertion sequence IS6110 (8).

* This work was supported, in whole or in part, by National Institutes of Health Grants AI052458 and AI33004 (to L. S. S.) and Contract NO1 AI-040091 (to J. T. B.). The costs of publication of this article were defrayed in part by the payment of page charges. This article must therefore be hereby marked "*advertisement*" in accordance with 18 U.S.C. Section 1734 solely to indicate this fact.

[S] The on-line version of this article (available at http://www.jbc.org) contains supplemental Figs. 1–4.

[1] To whom correspondence should be addressed: Center for Microbial Interface Biology, Dept. of Medicine, Division of Infectious Diseases, Ohio State University, 460 W. 12th Ave., Biomedical Research Tower, Rm. 1004, Columbus, OH 43210. Tel.: 614-292-8789; Fax: 614-292-9616; E-mail: larry.schlesinger@osumc.edu.

[2] The abbreviations used are: ManLAM, mannose-capped lipoarabinomannan; Ara, arabinose; DHB, 2,5-dihydroxybenzoic acid; dManLAM, deacylated ManLAM; GC, gas chromatography; HPAEC, high performance anion exchange chromatography; HSQC, heteronuclear single quantum correlation; LM, lipomannan; MDM, monocyte-derived macrophage; CR, complement receptor; MR, mannose receptor; PGG, principal genetic group; PGL, phenolic glycolipid; PIMs, phosphatidyl-*myo*-inositol mannosides; TEM, transmission electron microscopy; mAb, monoclonal antibody; Tricine, *N*-[2-hydroxy-1,1-bis(hydroxymethyl)ethyl]glycine; MALDI, matrix-assisted laser desorption/ionization; TOF, time-of-flight; MS, mass spectrometry.

Studies using this bank of clinical isolates showed that different *M. tuberculosis* clinical isolates within the PPGs vary in their ability to cause disease in humans and are capable of inducing different immunologic responses in the host. In particular, *M. tuberculosis* HN878 is associated with an unusually high proportion of active cases of disease and a high frequency of extrapulmonary disease (10). This has been attributed to immune subversion (14). In contrast, the *M. tuberculosis* clinical isolate CDC1551 caused a low number of cases of active disease, followed by an unusually high rate of seroconversion, and it has been found to induce a more rigorous immunologic response (9, 11).

Here we randomly selected *M. tuberculosis* strains from the bank of PGG-1, -2, and -3 *M. tuberculosis* isolates described above to screen for alterations in bacterial association with primary human macrophages in order to better characterize microbial determinants important in this process. We discovered that two phylogenetically related PGG-1 strains are significantly reduced in macrophage association and phagocytosis and demonstrate increased intracellular growth following serum opsonization. These strains contain a truncated form of ManLAM buried within their cell envelope and a reduction in higher order PIMs; thus, they do not engage the MR during phagocytosis. They also contain phenolic glycolipid (PGL), triglycerides and dimycocerosates, all known virulence factors (14–16). We propose a model for how distinct *M. tuberculosis* strains differ fundamentally in their macrophage interaction, a factor that may contribute to the increased representation of specific *M. tuberculosis* clones globally that impact the spectrum of human infections and disease.

EXPERIMENTAL PROCEDURES

Chemical Reagents and Antibodies—All chemical reagents were of the highest grade from Sigma unless otherwise specified. CS-35 and CS-40 murine monoclonal antibodies (mAbs) were kindly provided by both the Tuberculosis Research Materials and Vaccine Testing contract (NOI-AI-75320) and Leprosy Research Support contract (NOI-AI-25469).

Growth Conditions of M. tuberculosis Strains—Randomly selected *M. tuberculosis* clinical isolates (HN731, HN804, HN885, HN1390, HN1538, and HN1554 from PGG-1; HN657, HN703, and HN810 from PGG-2; and HN362 from PGG-3) were recovered from patients in Houston, TX, and characterized as described (8, 17). *M. tuberculosis* Erdman (ATCC 35801, within PGG-2) and $H_{37}R_v$ (ATCC 27294, within PGG-3) laboratory strains were also studied. Working stocks of all *M. tuberculosis* strains were grown on 7H11 plates and used as single suspensions, as described (18). Single cell suspensions were confirmed by high power light microscopy, repeating colony-forming unit (CFU) assays several times to correlate the numbers of bacteria counted in the Petroff-Hausser chamber with CFUs and performing tissue culture assays to ensure that the different clinical isolates settled comparably (similar buoyancies).

Isolation and Preparation of Human Macrophages—Monocyte-derived macrophage (MDM) monolayers were prepared from healthy tuberculin-negative human volunteers, as described (19). Monolayers (2×10^5 MDMs) for microscopy and CFUs were obtained by adherence to acid-washed glass coverslips or directly to plastic, respectively, in 24-well tissue culture plates for 2 h at 37 °C.

Assay of M. tuberculosis Association with MDMs—M. tuberculosis association assays with human MDM monolayers were performed as previously described (19). Briefly, MDM monolayers on coverslips in RPMI (BD Biosciences) containing 20 mM Hepes (RH) and 2.5% autologous human serum or RPMI containing 20 mM Hepes and 1 mg/ml human serum albumin (RHH) were incubated with *M. tuberculosis* single suspensions (2×10^6 bacilli) for 2 h at 37 °C in 5% CO_2. MDM monolayers were washed to remove nonassociated bacilli, fixed in 10% formalin, and washed again, and then associated *M. tuberculosis* bacilli were stained with auramine-rhodamine. The mean ± S.E. of cell-associated bacilli/MDM on triplicate coverslips was determined by counting ≥300 consecutive MDMs per coverslip using phase-contrast and fluorescence microscopy (19).

In some cases, MDMs were preincubated with anti-MR antibody (AbD Serotec, Raleigh, NC) at 10 μg/ml for 20 min at 37 °C to block the activity of the MR, as previously described (2, 3). For association with CR3 (complement receptor 3), CHO CR3 cells (1×10^5; provided by Douglas Golenbock, University of Massachusetts Medical School) were adhered to glass coverslips in 24-well tissue culture plates overnight at 37 °C and 5% CO_2. Washed monolayers were incubated with either *M. tuberculosis* strain Erdman or HN885 in either RH containing 2.5% human serum or RHH at 37 °C for 2 h. Infected monolayers were washed, fixed, and stained, and bacteria/cell was assessed as described above.

Transmission Electron Microscopy (TEM) of Strains Erdman and HN885 in Macrophages—M. tuberculosis bacilli (1×10^6) were added to MDM monolayers on glass coverslips and incubated for 2 h at 37 °C. Without washing, monolayers were fixed with 2.5% gluteraldehyde in 0.1 M sodium cacodylate buffer (pH 7.2) for 10 min, followed by 1 h in fresh fixative. Coverslip staining and TEM analysis of attachment and internalization of strains HN885 and Erdman by the macrophage was performed as previously described (19) using a Hitachi H-7000 transmission electron microscope. Five grids for each sample were analyzed by counting a total of 250–300 consecutive bacilli (~50 MDM cross-sections), and the ratio of intracellular *versus* extracellular surface-attached *M. tuberculosis* was determined.

Whole Cell ELISA for ManLAM on the M. tuberculosis Surface—Live *M. tuberculosis* single cell suspensions (5×10^5) were added to each well (triplicate wells) of a 96-well tissue culture plate and dried. Wells were blocked using 1% bovine serum albumin in phosphate-buffered saline with 0.05% Tween 20 for 2 h at room temperature, washed with phosphate-buffered saline containing 0.05% Tween 20, and incubated in either anti-LAM CS35 or CS40 mAb in 1% bovine serum albumin in phosphate-buffered saline overnight at room temperature. Then wells were washed and incubated with a secondary horseradish peroxidase-goat anti-mouse antibody (Bio-Rad) in 1% bovine serum albumin in phosphate-buffered saline for 2 h at room temperature. Plates were washed and developed using a peroxidase substrate kit (Bio-Rad). Reactions were stopped with 1% oxalic acid, and absorbance was measured at 405 nm. Three independent experiments were performed.

Total Lipid, ManLAM Purifications, Electrophoresis, Western Blotting, and Size Fractionation—Extraction of total lipids and ManLAM purifications were performed as previously reported (20). Pure ManLAM fractions were analyzed by electrophoresis using 10–20% gradient Tris/Tricine gels followed by periodic acid-silver staining. Sample concentrations were 0.5 μg/μl sample buffer. Western blotting using anti-LAM CS-35 and CS-40 mAbs (21, 22) was performed essentially as described (23) using a chemiluminescence system (Amersham Biosciences). Deacylation of ManLAMs and sizing chromatography using a 1 × 120-cm Bio-Gel P-100 (Bio-Rad) column were performed as previously described (24). Fractions were dried, and carbohydrate content was determined following the Dubois method (25).

Monosaccharide Composition and High Performance Anion Exchange Chromatography (HPAEC) Analyses—Samples were hydrolyzed with 2 M trifluoroacetic acid and converted to alditol acetates using *scyllo*-inositol as internal standard. Gas chromatography (GC) was performed as described (20). For HPAEC analyses, mixtures of ManLAM/LM from each strain were digested with endorabinanase and analyzed as previously described (20).

Matrix-assisted Laser Desorption/Ionization Time-of-flight (MALDI-TOF) MS Analyses—Analyses by MALDI-TOF MS were carried out on a Bruker Daltonic Reflex III (Bruker Daltonic) mass spectrometer. ManLAMs (0.5 μl of 10 μg/μl) were mixed with 0.5 μl of matrix solution (2,5-dihydroxybenzoic acid (DHB; 10 μg/μl) in a mixture of water/ethanol (1:1, v/v) and 0.1% trifluoroacetic acid) and air-dried. MALDI-TOF spectra were acquired in negative linear mode detection between 10,000 and 25,000 m/z and using a 300-ns time delay with a grid voltage of 80% of full accelerating voltage (25 kV) and guide wire voltage of 0.15%. For PIMs, MALDI-MS analyses were performed as previously described in positive mode (26).

NMR Spectrometry of ManLAMs—Two-dimensional ^{1}H-^{13}C heteronuclear single quantum correlation (HSQC) NMR spectra were obtained on a Bruker 600-MHz NMR spectrometer using the supplied Bruker pulse sequences. ManLAM samples were dissolved at 15 mg/ml in 100% D_2O as analytically quantified by GC analyses and lyophilized several times prior to experiments. HSQC data were acquired with a 7-kHz window for protons in F2 and a 15-kHz window for carbon in F1 with a total cycle time of 1.65 s between transients, as previously reported (20). Adiabatic decoupling was performed to carbon during proton acquisition. The final resolution was 3.5 Hz/point in F2 and 15 Hz/point in F1.

Intracellular Growth of Strains Erdman and HN885 in Macrophages—For measurements of intracellular growth in macrophages, 12-day-old MDM monolayers were washed, and *M. tuberculosis* bacilli were added to MDMs (multiplicity of infection 1:1; duplicate wells) in either RH containing 2.5% serum or RHH and incubated for 2 h at 37 °C in 5% CO_2 (27). Infected monolayers were washed and either repleted with RH containing 1% human autologous serum and further incubated for 24, 48, or 72 h or lysed (0 h time point) as described (27). After the 0 time point, the supernatant (containing detached infected MDMs) and monolayers were lysed separately and then pooled. Lysed samples were diluted, and then duplicates of three dilutions for each group were plated on 7H11 agar plates for 2–6 weeks (colony counts were identical within this interval). CFUs and doubling times were determined.

Statistical Analysis—Statistical analyses were performed using GraphPad Prism version 4.0 (available on the World Wide Web).

RESULTS

Association of M. tuberculosis Clinical Isolates with Primary Human Macrophages—We generated single cell suspensions (18), and using the same multiplicity of infection (10:1), we evaluated the macrophage association patterns of randomly selected strains from each of the three PGGs in the presence or absence of fresh nonimmune autologous serum. Fig. 1*A* shows a representative experiment for the association of HN885 and HN1554 clinical isolates *versus* the Erdman strain in the presence (*solid bars*) or absence (*open bars*) of serum. Our results showed that only strains HN885, HN1554, and, to a lesser extent, HN1538 were significantly reduced in macrophage association with or without serum relative to the control strain Erdman (Fig. 1*B*). Regardless of the PGG, all clinical isolates analyzed had a greater association (2–3-fold) with human MDMs in the presence of serum relative to the no serum condition (Fig. 1*B*), as previously shown for *M. tuberculosis* strains Erdman, $H_{37}R_v$ and $H_{37}R_a$ (19). To further analyze the result for the HN885 and HN1554 strains, we determined that the reduced association was observed regardless of the age of the bacterial culture used (standard 9 days *versus* 3 weeks) and the multiplicity of infection. Also, we determined that there was no difference in the degree of bacterial clumping or the stability of the bacterial phenotype (several serial passages on plates) (data not shown). Under all conditions, the reduction in bacterial association was greatest for strain HN885.

Receptor-mediated Phagocytosis for Strains Erdman, HN885, and HN1554—A highly expressed pattern recognition receptor on alveolar macrophages is the MR (28). We previously showed that the MR directly participates in the phagocytosis of virulent *M. tuberculosis* strains, defining a unique pathway for their intracellular trafficking (2, 19). Thus, we tested if the low association with human macrophages observed for HN885 and HN1554 was due to a deficiency in the recognition by the MR by using an anti-MR mAb (2, 3). Results in Fig. 2*A* show a representative experiment in the absence (*open bars*) or presence (*solid bars*) of anti-MR mAb, and results in Fig. 2*B* show combined data from three independent experiments. Whereas the association of strains Erdman and $H_{37}R_v$ with macrophages was significantly reduced when MDMs were pretreated with MR mAb (40.3 ± 8.4 and 47.8 ± 7.2%, respectively), the association of strains HN885 and HN1554 was minimally reduced in the presence of MR mAb (13.3 ± 8.2 and 5.1 ± 3.7%, respectively). Taken together, these data provide evidence that whereas strains Erdman and $H_{37}R_v$ engage the macrophage MR to optimize association with the macrophage (19), strains HN885 and HN1554 do not. The results suggested that these clinical isolates have an alteration(s) in their mannosylated cell wall molecules (*i.e.* reduction of ManLAM and higher order PIMs, both known MR ligands) that impaired their recognition by the MR.

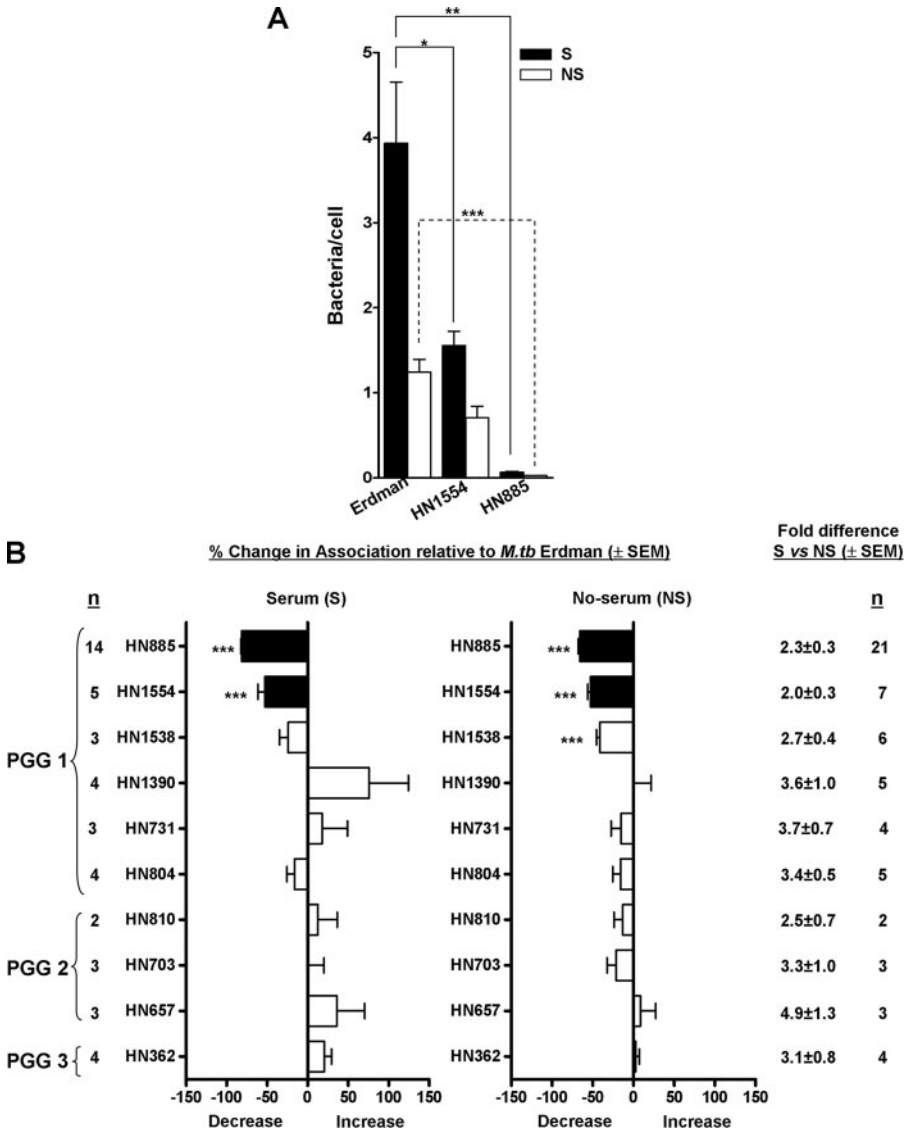

FIGURE 1. **Association of *M. tuberculosis* clinical isolates with human macrophages.** MDM monolayers were incubated with Erdman (reference strain) or the indicated *M. tuberculosis* (*M. tb*) clinical isolates in the presence (*S*) or absence (*NS*) of 2.5% serum for 2 h. Association was measured by phase-contrast and fluorescence microscopy. *A*, a representative association experiment for HN885 and HN1554 performed by triplicate in the presence or absence of serum. *B*, data represent percentage association of each clinical isolate relative to Erdman (*y* axis) for each condition (*n* is the number of independent experiments with the indicated isolate). *, $p < 0.05$; **, $p < 0.0005$; ***, $p < 0.0001$; Student's *t* test. The difference in bacterial association between the serum and no serum condition is depicted as summed data on the *right*.

CR3 is also a major receptor involved in *M. tuberculosis* phagocytosis by human macrophages in both the absence and presence (via C3 deposition) of serum (18). Our results show that there is no difference in the magnitude or nature of C3 fragment deposition on strains Erdman and HN885 or in the association with CR3 (supplemental Fig. 1).

We next studied whether the low association with macrophages observed for HN885 also translated into a defect in macrophage internalization (phagocytosis) of bacilli. Using TEM (19), we found that only under nonopsonic conditions (data for the opsonic condition is not shown) was there a significant difference (*, $p < 0.05$, $n = 3$) between Erdman and HN885 strains in that 89.6 ± 0.6% of strain Erdman was internalized after 2 h of infection, whereas only 58.0 ± 10.6% of strain HN885 was internalized (Fig. 2*C*). This result indicated that the defect in association observed for HN885 was also accompanied by a defect in phagocytosis under nonopsonic conditions, where the difference between strains HN885 and Erdman is in use of the MR by the latter strain.

Analysis of ManLAM on the Surface of Strains HN885 and HN1554—Since ManLAM is the major *M. tuberculosis* cell envelope ligand for the MR, we next assessed whether strains HN885 and HN1554 are deficient in cell surface exposure of ManLAM. ELISA and flow cytometry experiments were performed using anti-LAM mAbs (CS-35 and CS-40) (21, 22). The whole cell ELISA results using CS-35 and CS-40 (Fig. 2*D*) showed a significant reduction in the recognition of surface ManLAM on strains HN885 and HN1554 ($p < 0.0001$), a result confirmed by flow cytometry (supplemental Fig. 2). Analysis of cell lysates by SDS-PAGE and Western blot based on loading protein equivalents demonstrated that the ManLAM content was equivalent among all strains (data not shown). Thus, the reduced exposure of ManLAM observed on the surface of HN885 and HN554 appeared to be due to an alteration in their ManLAM structure and/or location.

Size and Molecular Composition of ManLAMs from Strains HN885 and HN1554—To examine for structural alterations present in ManLAMs from strains HN885 and HN1554, these were extracted and purified by size exclusion chromatography as we previously described (20). By Tris/Tricine-PAGE, HN885 and HN1554 exhibited a greater electrophoretic mobility, indicative of a smaller size (Fig. 3*A*). Western blot analysis confirmed this result and also showed all ManLAMs to react similarly to mAbs CS-35 and CS-40 (which recognize the terminal branched Ara_6 motif and the mannose-capped terminal arabinosyl epitopes of ManLAM, respectively; data not shown). To provide a different analytical perspective, Erdman, HN885, and HN1554 ManLAMs were deacylated by mild alkali treatment (dManLAM), and the size of their carbohydrate cores was determined on a P-100 sizing column. The three preparations generated different profiles (Fig. 3*B*). Erdman ManLAM eluted in earlier fractions (fractions 32–41) than the ManLAMs from HN885 (fractions 38–47) and HN1554 strains (fractions 39–48; data not shown) indicating that the carbohydrate cores of HN885 and

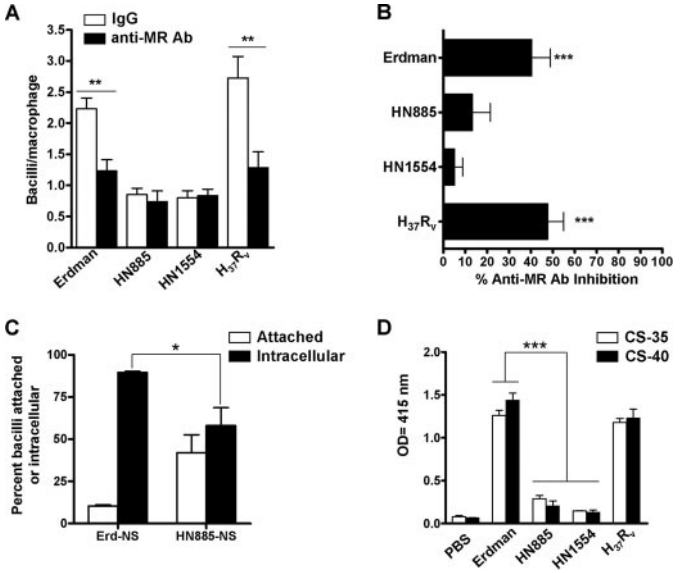

FIGURE 2. **Macrophage association (*A* and *B*), phagocytosis (*C*), and the exposure of ManLAM on the bacterial surface (*D*) for strains HN885 and HN1554.** *A*, a representative experiment performed in triplicate in which MDM monolayers were preincubated with 10 μg/ml anti-MR mAb (*solid bars*) or IgG1 isotype (*open bars*) before incubation with the *M. tuberculosis* strains. **, $p < 0.005$; Student's *t* test. The results show that HN885 and HN1554 do not use the MR to associate with human macrophages, and the overall MR-dependent association of *M. tuberculosis* strains with MDMs is represented by percentage inhibition in the presence of anti-MR mAb relative to the subtype control mAb (*B*). ***, $p < 0.0001$; one-way analysis of variance Tukey post-test clinical isolates *versus M. tuberculosis* control strains (Erdman/$H_{37}R_v$), $n = 6$. *C*, percentage of *M. tuberculosis* Erdman and HN885 attached *versus* internalized (phagocytosed) by macrophages. MDM monolayers on glass coverslips were incubated with Erdman or HN885 *M. tuberculosis* in the presence or absence of 2.5% serum for 2 h, fixed, and prepared for TEM analysis. Data represent mean ± S.E. (*, $p < 0.05$, $n = 3$ by triplicate) for the percentage of bacteria that were intracellular *versus* extracellular. *D*, ManLAM detection on the surface of *M. tuberculosis* strains. Whole bacterial ELISA using live *M. tuberculosis* and anti-LAM mAb CS-35 shows a significant reduction in the recognition of surface ManLAM on strains HN885 and HN1554 (***, $p < 0.001$; one-way analysis of variance, Tukey post-test, clinical isolates *versus* control strains (Erdman/$H_{37}R_v$), $n = 3$ by triplicate).

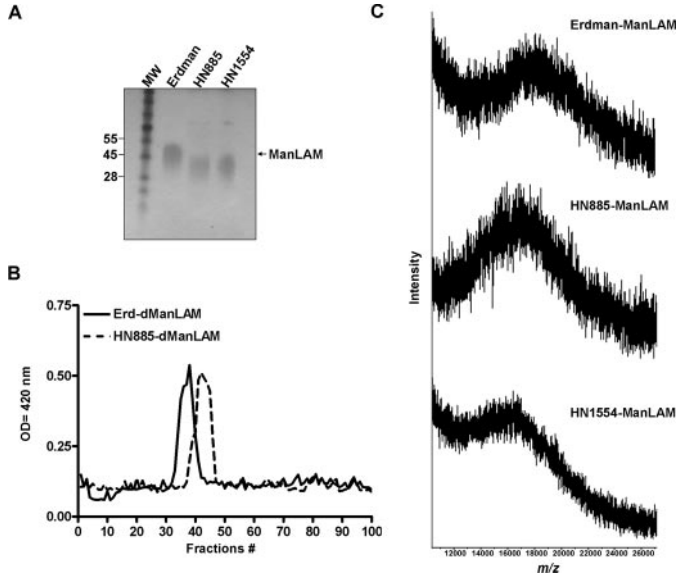

FIGURE 3. **Size of ManLAMs from *M. tuberculosis* strains.** *A*, 10–20% gradient Tris/Tricine gel followed by periodic acid-silver staining shows that ManLAMs from strains HN885 and HN1554 exhibit a greater electrophoretic mobility than ManLAM from strain Erdman; the size difference can be approximated by aligning the respective leading edges of the characteristic broad electrophoretic bands. *MW*, molecular weight. *B*, sizing column chromatography of deacylated ManLAMs. After deacylation, 1 mg of dManLAM was loaded onto a P-100 sizing column, and 1-ml fractions were collected, dried, and analyzed by carbohydrate content. Erd-dManLAM (*solid line*) eluted earlier from the column than HN885-dManLAM (*interrupted line*), indicating that its carbohydrate core is larger. *C*, negative MALDI mass spectrum of Erdman, HN885, and HN1554 ManLAMs. ManLAM (0.5 μl of a 10 μg/μl solution) was mixed with 0.5 μl of the matrix solution (10 μg/μl) of DHB in ethanol/water (1:1, v/v) and analyzed by MALDI-TOF in the negative mode.

TABLE 1

ManLAM carbohydrate composition analysis of different *M. tuberculosis* strains

Analyses of the alditol acetates derivatives were determined by GC/MS. Values represent mean; $n = 3$ by duplicate.

	Ara	Man	*myo*-Inositol	Ara/Man ratio
M. tuberculosis Erdman	56	49	1	1.14
M. tuberculosis $H_{37}R_v$	56	55	1	1.02
M. tuberculosis HN885	32	27	1	1.18
M. tuberculosis HN1554	45	44	1	1.02

HN1554 ManLAMs were smaller. The size variation observed for HN885 and HN1554 ManLAMs was further estimated by MALDI-TOF MS. The negative MALDI-TOF MS spectrum of Erdman ManLAM showed a broad unresolved peak centered at *m/z* 18,500 (Fig. 3*C*), indicating a molecular mass of ~18.5 kDa, the major molecular species observed for this lipoglycan (29). Analysis of ManLAMs from HN885 and HN1554 (Fig. 3*C*) revealed a smaller average molecular mass of ~16.5 and 15.0 kDa, respectively (Fig. 3*C*). ManLAM monosaccharide composition analysis by GC showed an arabinose (Ara*f*) to mannose (Man*p*) ratio of 1.18 and 1.02 to 1 for strains HN885 and HN1554, respectively, which is comparable with those of strain Erdman and $H_{37}R_v$ ManLAMs (Table 1). However, when neutral sugar composition was quantified based on 1 inositol/mol of ManLAM, strain HN885 ManLAM yielded 32 Ara*f* and 27 Man*p* residues compared with 56 Ara*f* and 49 Man*p* residues for ManLAM from strain Erdman. Similar differences (fewer Ara*f* and Man*p* residues) were observed for the ManLAM from strain HN1554, also consistent with its smaller size (Table 1). Thus, the absolute neutral sugar composition is in support of an overall smaller size for HN885 and HN1554 ManLAMs, consistent with their greater migration by Tris/Tricine-PAGE, their P-100 column elution profiles, and their MALDI-TOF MS spectra.

Erdman, HN885, and HN1554 ManLAM fatty acid composition was also determined by GC/MS after methanolysis and trimethylsilylation (20). The ions at *m/z* 270 and 312, which correspond to hexadecanoic acid ($C_{16:0}$) and Δ10-methyloctadecanoic acid (C19 or tuberculostearic acid), respectively, were found in all ManLAMs. In addition, both HN885 and HN1554 contained an octadecanoic acid ($C_{18:0}$, *m/z* 298) (data not shown).

Enzymatic Digestion and Methylation Analysis of ManLAMs—Enzymatic digestion of arabinan by *Cellulomonas* endoarabinanase has been used as a means to analyze specifically the nature of the nonreducing termini of ManLAM (30). Erdman, HN885, and HN1554 ManLAMs were digested with endoarabinanase, and the products were analyzed by Dionex-HPAEC. The HPAEC profile of the digested ManLAM of strain Erdman revealed three major characteristic oligosaccharide peaks (Ara_2 (representative of the internal regions of the arabinan) and

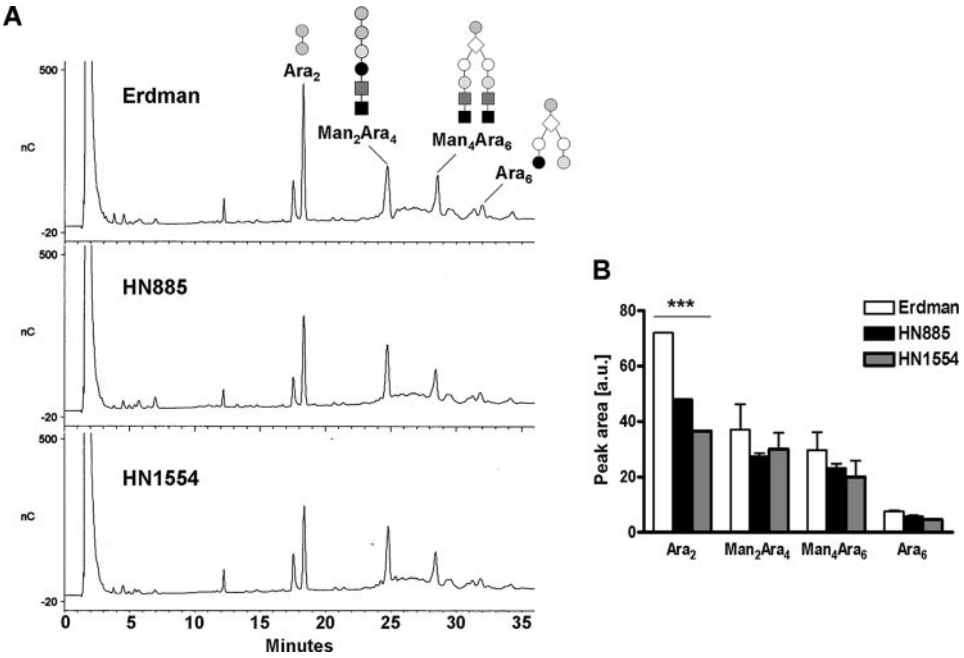

FIGURE 4. **HPAEC profile of endoarabinanase-digested *M. tuberculosis* ManLAMs.** *A*, representative HPAEC profiles for Erdman, HN885, and HN1554 ManLAMs. For direct comparison, the digestion products were dried and injected directly without further purification. Ara_2 and Man_2Ara_4 are linear oligosaccharides, whereas Ara_6 and Man_4Ara_6 are branched. *B*, quantification of the peak areas observed by HPAEC analysis. Values represent mean ± S.E. ($n = 2$) by duplicate. ***, $p < 0.0001$; Student's *t* test, clinical isolates *versus* control strain Erdman.

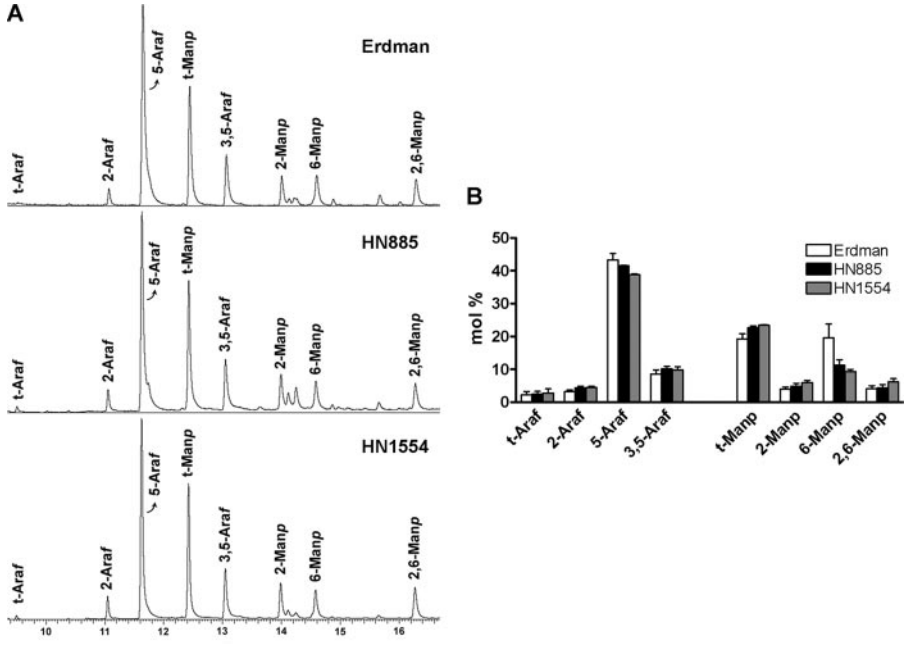

FIGURE 5. **Linkage analysis of *M. tuberculosis* ManLAMs as determined by GC/MS.** Samples were per-*O*-methylated, hydrolyzed, reduced, and acetylated, and partially methylated alditol acetates were analyzed by GC/MS as described under "Experimental Procedures." *A*, the spectra of various linked Ara and Man derivatives in the ManLAMs from Erdman, HN885, and HN1554 are shown. *B*, the *bar graph* shows calculated mol % of specific linked sugars in the purified ManLAMs. Values represent mean ± S.E. ($n = 2$) by duplicate.

Man_2Ara_4 and Man_4Ara_6 (both representative of the linear and branched nonreducing termini of ManLAM-arabinan, respectively)) and a much smaller peak for the non-mannose-capped Ara_6 (Fig. 4*A*). However, HN885- and HN1554-digested ManLAM HPAEC profiles (Fig. 4*A*) showed a significant reduction in the relative abundance of the ManLAM-derived Ara_2 fragments (a decrease of 33.0 and 49.3% for HN885 and HN1554, respectively), indicating a size reduction in their arabinans. An overall reduction in the amounts of Man_2Ara_4, Man_4Ara_6, and Ara_6 fragments (especially Man_4Ara_6) was also observed when compared with those of strain Erdman (Fig. 4*B*). Subsequent treatment of the endoarabinanase-treated material with α-mannosidase confirmed the identity of the mannose-capped Ara_4 and Ara_6 fragments (data not shown).

Linkage analysis was also performed to further examine differences in the arabinan and mannan structures within the ManLAMs of these strains. The permethylated alditol acetate profiles of Erdman, HN885, and HN1554 ManLAMs were established by GC/MS (Fig. 5*A*). The *bar graph* in Fig. 5*B* reflects the linkage compositional analysis of all ManLAMs based on areas under the curve for each sugar type detected by GC/MS. Three major conclusions were derived from this experiment. First, the content of 5-Ara (5-αAra + 5-βAra) is lower in both clinical isolate ManLAMs. This result corresponds directly with the decrease in Ara_2 observed for the Dionex-HPAEC profiles, where Ara_2 is exclusively defined as Ara*f*-α(1→5)-Ara*f* disaccharide. The fact that the decrease in 5-Ara by methylation analysis is not as marked as the decrease observed for Ara_2 by HPAEC analysis can be explained by the fact that both clinical isolate ManLAMs are more branched in their arabinan domain (*i.e.* contain more 3,5-Ara) (Fig. 5*B*). Previous structural analysis (31, 32) showed that for each 3,5-Ara, there are two 5-β-Ara residues (for mannose-capped branches only). Because we cannot differentiate among α- and β-isomers by linkage analysis, the slight increase of 5-β-Ara in the clinical isolate ManLAMs masks the decrease of 5-α-Ara observed by our HPAEC experiments. The presence of more 5-β-Ara in both clinical isolate ManLAMs could also be explained by both ManLAMs having greater values for the residues related to their mannose caps (*i.e. t*-Man and 2-Man). Methylation analysis does not allow us to exclude this possibility, since *t*-Man and 2-Man can also be related to the mannan

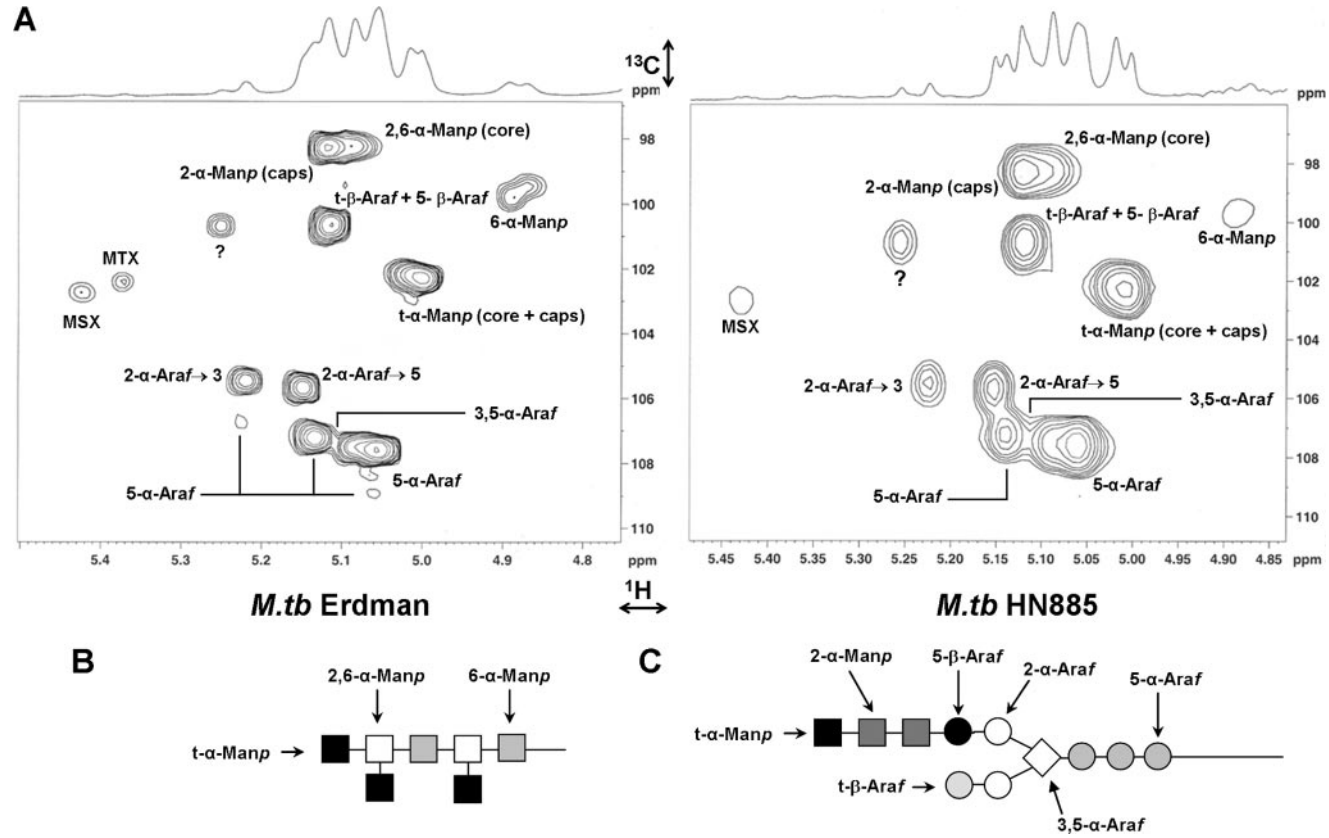

FIGURE 6. **Comparative partial two-dimensional NMR spectra of Erdman and HN885 ManLAMs.** *A*, two-dimensional NMR ^{1}H-^{13}C HSQC spectra were acquired in D_2O. Only the expanded anomeric regions are shown. ?, unidentified peaks. The intensity of peak volumes was measured, and the data are presented in Table 2. Shown are representations of the sugar linkages described for the mannan (*B*) and arabinan (*C*) domains of ManLAM. *M. tb*, *M. tuberculosis*.

domain of ManLAM. Second, the content of 6-Man was markedly reduced in both clinical isolates, where 6-Man defines the linear mannan core of ManLAM.

The third and most interesting conclusion is that all of the differentially linked Ara*f* and Man*p* residues were present in all of the ManLAMs analyzed, and their relative ratios did not change significantly, indicating that both HN885 and HN1554 ManLAMs have a reduction in their arabinan and mannan content, while retaining their basic structure as observed for Erdman.

Structural Features of ManLAMs—To further uncover the exact chemical composition of the clinical isolate ManLAMs, the different NMR spin systems of Erdman, HN885, and HN1554 ManLAMs were further characterized by one-dimensional ^{1}H and two-dimensional ^{1}H-^{13}C HSQC NMR (Fig. 6*A*). The assignment of the resonances in a one-dimensional ^{1}H NMR can be challenging, since the protons are in a strong overlapping region of the spectrum. However, as previously reported (33), this approach allowed us to identify two intense broad triplets centered between δ2.5 and δ2.65 ppm, which were attributed to the methylene of the succinyl groups located in the C-2 of the branched 3,5-Ara*f* in the ManLAM arabinan (33) (data not shown). Upon deacylation, the resonances for succinates and fatty acids (δ2.65–0.5) were removed, indicating their covalent ester bonds (20).

Resonances related to the overlapping anomeric region can be better resolved by two-dimensional ^{1}H-^{13}C HSQC NMR experiments. As highlighted in previous studies (31, 34), the carbohydrate backbone of ManLAM is composed of an α(1→6)Man*p* backbone substituted at most of the O-2-positions by *t*-Man*p* units (Fig. 6*B*). Our methylation analysis revealed that the mannan domain of the clinical isolate ManLAMs is composed of *t*-Man*p*, 6-Man*p*, and 2,6-Man*p*, corresponding to the mannan core, and *t*-Man*p* and 2-Man*p*, corresponding to the mannose caps. By comparing the ^{1}H-^{13}C HSQC NMR spectra from the HN885, HN1554, and Erdman ManLAMs and in agreement with our previous work (20), the spin systems of all mannose types could be determined (Table 2). Spectral data on different ManLAMs were acquired on separate days, and the chemical shift changed by 0.1–0.3 ppm. Chemical shifts for Erdman ManLAM were taken as a generic standard for analysis of the HN885 and HN1554 ManLAMs. Both clinical isolate ManLAMs demonstrated an overall reduction in their spin systems related to their mannan domain. However, when the 2,6-α-Man*p*/(2,6-α-Man*p* + 6-α-Man*p*) ratio (29) was calculated from the H-1 signal integration values, a degree of branching of 70, 80, and 87% for Erdman, HN885, and HN1554, respectively, was obtained. These data are in agreement with the difference in the degree of branching determined by our methylation analysis (*i.e.* 11 and 21% increase in branching in the HN885 and HN1554 mannan cores, respectively, when compared with Erdman). A marked difference between both clinical isolates and Erdman was also observed for the spin system corresponding to 6-α-Man*p* (δ102.2, δ5.00), where HN885 and HN1554 showed a 2.6- and 1.4-fold decrease, respectively, when compared with Erdman Man-

TABLE 2

Anomeric resonances of ManLAMs from different *M. tuberculosis* strains

Signal volumes were determined from ^{1}H-^{13}C HSQC NMR experiments consecutively performed using the same Bruker 600-MHz NMR spectrometer.

Residues	^{13}C	^{1}H	ErdLAM volume[a]	HN885LAM volume[a]	HN1554LAM volume[a]
2,6-α-Man*p* (core)	98.4	5.06	6.00	2.60	4.32
2-α-Man*p* (caps)	98.2	5.13	11.20	4.63	4.19
6-α-Man*p*	99.4	4.86	2.48	0.68	0.64
t-β-Ara*f* + 5-β-Ara*f*	100.6	5.10	10.50	4.52	4.61
t-α-Manp (core + caps)	102.2	5.00	16.80	7.03	8.77
MTX[b]	102.4	5.37	0.47	0.18	0.29
MSX[c]	102.7	5.42	0.60	0.46	0.51
2-Ara*f*→3	105.4	5.21	2.95	1.18	1.20
2-Ara*f*→5	105.6	5.14	10.50	4.52	4.61
5-α-Ara*f*	106.7	5.22	0.45	0.39	0.13
5-α-Ara*f*	107.2	5.15	8.97	3.52	3.75
3,5-α-Ara*f*[d]	107.4	5.11	1.45	0.48	0.46
5-α-Ara*f*	107.6	5.04	35.25	13.94	16.05
5-α-Ara*f*	109.4	5.05	0.22	0.20	0.12

[a] Signal volumes were normalized and integrated to a reference signal located at ^{13}C, ^{1}H (δ100.05, δ5.22) common to all of the ManLAMs studied.
[b] 5-methyl-5-thio-α-xylofuranose.
[c] 5-deoxy-5-methyl-5-sulfoxy-α-xylofuranose.
[d] There is a significant overlap in 3,5-α-Ara*f* with 5-α-Ara*f*, and thus the integration of signal volumes of 3,5-α-Ara*f* cannot be unambiguously assigned. This is one explanation for a lower value of this peak in this table.

LAM. Thus, in comparison with Erdman ManLAM, both clinical isolates had a shorter mannan core with a higher degree of branching.

Although overlapping anomeric signals for *t*-α-Man*p* ($\delta C_1$102.2, $\delta H_1$5.00) were assigned to both the mannan core and mannose caps, and these were less prominent in both clinical isolates, the *t*-α-Man*p*/(*t*-α-Man*p* + 2-Man*p*) ratio indicated no marked differences in their degree of mannose capping or the lengths of mannose caps (*i.e.* mono-, di-, or trimannosides) when compared with Erdman ManLAM (*i.e.* ~60% for Erdman and HN885 and 68% for HN1554). This result is also in agreement with our methylation analysis, where a slight increase in the degree of mannose capping was only observed for HN1554 ManLAM.

As observed previously for mycobacterial LAMs, some Ara units with identical spin systems had multiple H-1 signals that led to the assignment of one 3,5-α-Ara*f* volume, four 5-α-Ara*f* volumes, two 2-α-Ara*f* volumes, and a single *t*-β-Ara*f* + 5-β-Ara*f* volume for Erdman ManLAM, representing the different positions that each Ara unit may have within the arabinan domain (Fig. 6*C*). Consistent with our previous results (20), the HSQC spectrum for Erdman ManLAM presented a series of spin signals attributed to 5-α-Ara*f* and 3,5-α-Ara*f*. In both HN885 and HN1554 ManLAMs, these signals (especially the spin volume for 5-α-Ara*f* (Table 2)) were markedly reduced, indicating a shorter linear (Ara*f*-α(1→5)-Ara*f*) backbone chain in their arabinan domains. This observation correlates with our methylation and HPAEC analyses, where both clinical isolates had a marked decrease in their 5-Ara residue, indicating a prominent size reduction in their linear arabinan domain.

Two spin systems were also identified for 2-α-Ara*f*, those attached to the 3-position (2-α-Ara*f*→3, δ105.4, δ5.21) and 5-position (2-α-Ara*f*→5, δ105.6, δ5.14) of the 3,5-α-Ara*f* (δ107.4, δ5.11). As expected, the intensity of 2-α-Ara*f*→5 signal was stronger than that of 2-α-Ara*f*→3 due to the lack of substitution in the C-3-position, which results in the terminal linear Ara_4 motif. Although both volumes were smaller in the clinical isolate ManLAMs, the ratios 2-α-Ara*f*→5/(3,5-Ara*f* + 2-α-Ara*f*→5) and 2-α-Ara*f*→3/(3,5-Ara*f* + 2-α-Ara*f*→3) indicated a slight increase in their branching patterns when compared with Erdman arabinan.

The chemical shifts at C_1δ100.6 and H_1δ5.10 corresponded to the terminal β-Ara*f* with overlapping 5-β-Ara*f*, and their volumes were also smaller in both clinical isolates when compared with Erdman ManLAM. In the NMR spectra, the anomeric signals for *t*-β-Ara*f* and 5-β-Ara*f* had a perfect overlap; however, the substitution on the 5-OH by the mannose caps results in a significant shift at the C-5 of the β-Ara*f* (20). From the same ^{1}H-^{13}C HSQC NMR spectra, detailed analysis of the hydroxymethylene region showed that all ManLAMs had 5-β-Ara*f* with a similar ratio for C-5 of 5-β-Ara*f*/t-β-Ara*f*, indicating a similar amount of *t*-β-Ara*f* in all ManLAMs (data not shown). Similar results were obtained by methylation analysis with a *t*-Ara ratio of 0.92:1.00:1.13 for Erdman, HN885, and HN1554 ManLAMs, respectively. The recently defined signal corresponding to a 5-methyl-5-thio-α-xylofuranose residue was observed in Erdman and $H_{37}R_v$ ManLAMs only. However, its corresponding oxidized counterpart, 5-deoxy-5-methyl-5-sulfoxy-α-xylofuranose, was observed in all of the ManLAMs studied (35).

Thus, the data derived from the ^{1}H-^{13}C HSQC NMR spectra, together with the methylation and HPAEC analyses, provide evidence that the ManLAMs from clinical isolates HN885 and HN1554 have a decrease in their ManLAM length with a notable truncation of their linear arabinan (*i.e.* decrease of 5-α-Ara*f*) and mannan (*i.e.* decrease of 6-α-Man*p*) domains, with the latter highly substituted by *t*-Man*p* and/or several shorter arabinan chains. However, we can rule out the possibility of multiple shorter arabinan chains, since our results do not support these structures in all *M. tuberculosis* ManLAMs studied (*i.e.* high values for 2-α-Ara*f* and 3,5-α-Ara*f* relative to the decrease of 5-α-Ara*f* observed).

Total PIM Content in the Cell Envelope of Strains Erdman, HN885, and HN1554—In addition to ManLAM, we recently showed that higher order PIMs on the cell surface of virulent *M. tuberculosis* strains also associate with the MR during phagocytosis and contribute to the mycobacterial phagosome matu-

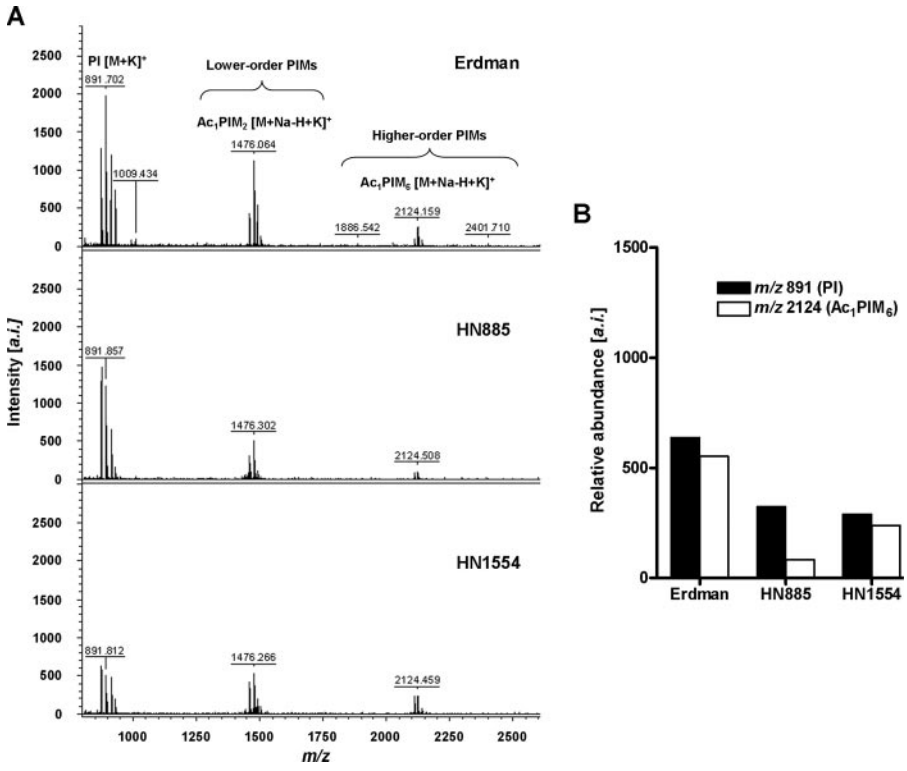

FIGURE 7. **Total PIM analysis of *M. tuberculosis* strains by MALDI-TOF.** *A*, the MALDI-TOF mass spectra of the total PIM extract from strains Erdman, HN885, and HN1554. Cell lysates (500 μg normalized by protein content) from each strain were extracted with chloroform/methanol (2:1, v/v) for 12 h, followed by chloroform/methanol (1:2, v/v) for an additional 12 h. Extracts were dried down and precipitated in cold acetone for 12 h. PIMs were mixed with DHB matrix in chloroform/methanol/water (10:10:3, v/v/v) and analyzed by MALDI-TOF in the positive mode. Major differences in lower and higher order PIM content were observed among the *M. tuberculosis* strains, where strains HN885 and HN1554 contain significantly fewer higher order PIMs than strain Erdman. *a.i.*, arbitrary intensity. *B*, quantification of PIMs by MALDI-TOF MS. Samples were co-crystallized with DHB matrix on the probe using solvent evaporation, desorbed and ionized by a nitrogen laser pulse (337 nm), and then accelerated under 25 kV with time-delayed extraction before entering the time-of-flight mass spectrometer. The number of laser pulses was received as 3 $\times$ 60 or 180 laser pulses for a final MALDI-MS spectrum. Samples with and without the standard (α(1→4)-mannobiose, M_r 342.30) were mixed with the matrix (1:1, v/v). For the individual PIMs identified, summation of all ion responses occurred ($[M + Na]^+$ plus $[M + K]^+$ plus $[M + Na\text{-}H + K]^+$). Values represent mean of a representative experiment by triplicate ($n = 3$).

ration arrest (3). Thus, we analyzed the total PIM composition on the cell envelope of HN885 and HN1554 to determine if their reduction might be another reason for low association with the MR. Total PIMs were extracted and analyzed by MALDI-TOF MS (Fig. 7) and two-dimensional TLC (supplemental Fig. 3). Results show that all strains contained all of the predicted PIMs, and there were no differences in their acylation patterns. Fig. 7*A* shows the total PIM MALDI-TOF MS spectra for Erdman, HN885, and HN1554 strains. Three major signals were determined. *m/z* 891.7 can be assigned as $[M + K]^+$ for phosphatidyl-*myo*-inositol with palmitic ($C_{16:0}$) and tuberculostearic acids on the C-1- and C-2-positions of the glycerol. The signal *m/z* 1476.0 can be assigned as $[M + Na\text{-}H + K]^+$ for Ac_1PIM_2 (a lower order PIM) with an additional $C_{16:0}$ either on the C-6-position of the α(1→2)-linked mannose or on the C-3 of the *myo*-inositol (36). The signal at *m/z* 2124.5 corresponding to $[M + Na\text{-}H + K]^+$ of Ac_1PIM_6, a higher order PIM that engages the MR and contributes to the limited phagosome-lysosome fusion (3), was also observed. Our results by MS (Fig. 7*B*), corroborated by densitometry on the two-dimensional TLC (supplemental Fig. 3), indicate that HN885 and HN1554 clinical isolates have a decrease in terminal α2-Man*p* of their PIMs when compared with strain Erdman.

In addition to PIMs, strains HN885 and HN1554 also contained abundant pthiocerol dimycocerosates, triglycerides (supplemental Fig. 4*A*) and PGL (supplemental Fig. 4, *B* and *C*) in their cell envelope, all known *M. tuberculosis* virulence factors (14–16). These were not observed in the laboratory strain Erdman. Thus, we speculate that the presence of pthiocerol dimycocerosates, triglycerides, and PGL in these clinical isolates, in addition to their truncated form of ManLAM and their general decrease in higher order PIMs, may serve to further mask the already low content of surface-exposed terminal α(1→2)-Man, explaining the poor recognition of these clinical isolates by the human macrophage MR.

Intracellular Growth of Strains Erdman and HN885—There is increasing evidence that the use of a specific receptor(s) on the surface of the human macrophage by *M. tuberculosis* can dictate the outcome of *M. tuberculosis* infection (37). Here we show that HN885 and Erdman differ in their use of the MR during phagocytosis. Therefore, to determine whether this difference would lead to differences in their intracellular growth in macrophages, MDMs were incubated with each strain, CFU assays were performed, and doubling times in macrophages were calculated. Results show that for nonopsonized bacilli (no serum), the doubling time for strain HN885 was the same as for Erdman (Table 3). In contrast, following serum opsonization, the doubling time for strain HN885 was reduced when compared with Erdman (Table 3). Thus, although reduced in phagocytosis, and therefore less internalized for a given multiplicity of infection (Fig. 2, *A*–*C*), those strain HN885 bacilli that do enter macrophages divide more rapidly than the *M. tuberculosis* Erdman strain, a finding that is most evident after serum opsonization.

DISCUSSION

Continued efforts to define the molecular events in the early interaction between *M. tuberculosis* and the human macrophage are necessary to further understand the immunopathogenesis of tuberculosis and disease outcome. This study has identified two *M. tuberculosis* strains (*i.e.* HN885 and HN1554) among a bank of *M. tuberculosis* clinical isolates (8, 17) with a striking defect in phagocytosis by primary human macrophages

TABLE 3

Doubling time for *M. tuberculosis* strains Erdman and HN885 in macrophages

MDM monolayers were incubated with strain Erdman or HN885 for 2 h in the absence (NS) or presence (S) of 2.5% serum. CFU were measured 2–6 weeks after plating, and the doubling times were calculated. Results represent mean ± S.E. for $n = 2$.

Strain	Condition	24 h	48 h	72 h
Erdman	NS	10.8 ± 3.8[a]	25.5 ± 12.9	24.7 ± 7.8
HN885	NS	12.8 ± 5.8	23.4 ± 12.5a	20.6 ± 6.4a
Erdman	S	24.6 ± 15.9	46.1 ± 31.1	29.3 ± 10.8
HN885	S	16.2 ± 8.6a	20.7 ± 8.2a	24.8 ± 9.6a

[a] Shorter time indicates faster replication within human macrophages.

when compared with strain Erdman, a commonly used laboratory strain for studies of pathogenesis. The defect in phagocytosis was found to result from significant alterations in the mannosylated cell envelope components of these strains that impact recognition by the macrophage MR and intracellular bacterial survival.

ManLAM is a predominant lipoglycan of the *M. tuberculosis* cell envelope that has been found to play a central role in the virulence and immunopathogenesis of tuberculosis (38). ManLAM and higher order PIMs (*i.e.* PIM_5 and PIM_6), mediate phagocytosis of bacilli by human macrophages via the MR, resulting in limited phagosome-lysosome fusion events for this bacterium (2, 3). The cell biological effects of ManLAM are numerous and are the focus of research in a number of laboratories (reviewed in Ref. 37). In many cases, these biological effects are linked to the nature and extent of the mannose capping as well as to other substitutions in the arabinan chains. To date, ManLAM structures have been determined from only a limited number of *M. tuberculosis* strains. Here we provide the first report of two clinical isolates of *M. tuberculosis* that do not expose ManLAM on their surface. This is not due to a difference in their total ManLAM content when compared with the Erdman and $H_{37}R_v$ strains but rather to a difference in the structure and location of the ManLAMs from these isolates.

When purified ManLAMs were subjected to rigorous biochemical analysis, our results demonstrated that strains HN885 and HN1554 contain an overall shorter and in several respects simpler ManLAM (Fig. 8*A*). Specifically, our sugar analysis and HPAEC, methylation, and NMR analyses showed that ManLAM molecules from HN885 and HN1554 have a marked reduction in Ara*f* residues, which corresponds mainly to the inner Ara*f*-α(1→5)-Ara*f* (known as Ara_2) unit of the arabinan domain. Our results also indicate that both HN885 and HN155 arabinans are composed of a limited number of short arabinose chains (*i.e.* 1–2 chains per ManLAM molecule). In addition, the mannan domain of their respective ManLAMs is altered, with fewer 6-Man*p* residues, indicating a shorter but more substituted linear Man*p*-α(1→6)-Man*p* unit (Fig. 8*A*). The structurally truncated ManLAM molecule produced by HN885 and HN1554 probably reduces its surface availability.

To date, truncated ManLAMs have only been observed in *M. tuberculosis* ethambutol-resistant strains under laboratory conditions (20, 39); in contrast, the *M. tuberculosis* strains reported here are all ethambutol-susceptible (data not shown). We also found that there was a marked reduction of higher order PIMs. Less exposed ManLAM and reduced higher order

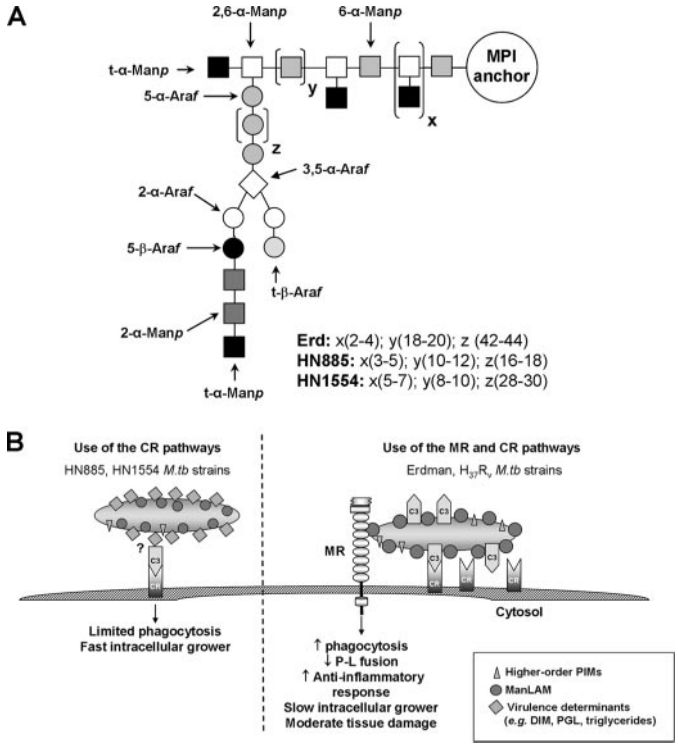

FIGURE 8. **A proposed model for HN885 and HN1554 ManLAM structures (*A*) and a proposed model for routes of entry and consequences for *M. tuberculosis* HN885 and HN1554 strains in human macrophages (*B*).** Representation of HN885 and HN1554 ManLAMs (*A*), where *x* and *y* represent the number of branches and number of 6-α-Man*p* residues present in the mannan core, respectively. Erdman ManLAM has a longer (18–20 6-α-Man*p* residues) mannan domain when compared with HN885 and HN1554 (with 10–12 and 8–10 6-α-Man*p* residues, respectively). In addition, *z* represents the number of 5-α-Ara*f* residues that form the linear arabinan domain of ManLAM. Based on our results, this value was estimated to be about 42–44 for Erd-ManLAM, whereas in the case of HN885 and HN1554, it is estimated to be 16–18 and 28–30, respectively, indicating that both clinical isolates have a shorter linear arabinan domain in their respective ManLAMs. *B*, proposed model for entry and subsequent consequences for HN885 and HN1554 strains in human macrophages. *M. tuberculosis* strains HN885 and HN1554 have reduced surface exposure of ManLAM and do not use the MR pathway during phagocytosis. These strains contain pthiocerol dimycocerosates, triglycerides, and PGL and demonstrate limited phagocytosis primarily via the C3-CR3 pathway and rapid intracellular growth. In contrast, *M. tuberculosis* Erdman and $H_{37}R_v$ strains heavily coat their surface with mannose residues, including a more complex ManLAM, and increased amounts of higher order PIMs, which promote phagocytosis by the MR pathway in concert with CRs. These highly mannosylated strains subvert the host immune response; however, they are more host-adapted, and infection is associated with less tissue damage and slower intracellular growth.

PIMs translated to a low association of these clinical isolates with the MR and reduced phagocytosis by human macrophages as seen in our TEM studies.

It is also possible that the ManLAMs from strains HN885 and HN1554 have a less favorable spatial conformation for engaging the MR; however, we reason that their ManLAMs have the same spatial flexibility in their carbohydrate domains, as indicated by their Ara*f*/Man*p* ratio values, which are similar to the Erdman and $H_{37}R_v$ strains (Table 1). In addition, we found that strains HN885 and HN1554 have abundant dimycocerosates, triglycerides, and, to a lesser extent, PGL, in their cell envelopes. We speculate that the presence of these molecules further masks the exposure of ManLAM and the higher-order PIMs. Overall, our data indicate that low binding to the MR is a direct consequence of a significant reduction in α(1→2) mannosy-

lated surface-exposed components in the cell envelope of these clinical isolates.

Strains HN885 and HN1554 displayed normal C3 opsonization and interaction with host cell CR3 (supplemental Fig. 1). However, these results do not exclude the possibility that the binding to other CRs (*e.g.* CR1 and CR4 (40)) may be altered. Our results are consistent with the idea that CRs cooperate with the MR for optimal phagocytosis by macrophages. Akin to other models of lectin/integrin interactions, the MR may be particularly important in enhancing the initial adhesion of bacteria to macrophages prior to efficient internalization mediated by itself and/or the CRs. Finally, although the MR and CRs are the main phagocytic receptors described for *M. tuberculosis* on primary human macrophages, other receptors for *M. tuberculosis* phagocytosis have been described (reviewed in Ref. 37), which may be altered in their interaction with these clinical isolates and were not the focus of the current study.

Our data show that despite the decrease in macrophage phagocytosis of HN885 (Fig. 2*C*) and consequently the number of intracellular bacteria, the intracellular growth rate (expressed as doubling time; Table 3) for those HN885 bacilli that do enter macrophages is similar to Erdman in the absence of serum and faster (shorter doubling time) than Erdman in the presence of serum. This suggests that the mechanisms for intracellular survival and growth of HN885 (and potentially for other clinical isolates) following phagocytosis are fundamentally different from the ones described for Erdman and $H_{37}R_v$ (reviewed in Ref. 37) and worthy of further study.

Our results lead us to propose a new model for the phagocytosis of *M. tuberculosis* strains by human macrophages (Fig. 8*B*). *M. tuberculosis* strains that have less surface mannosylation do not use the MR during phagocytosis. Such strains are reduced in phagocytosis, relying primarily on C3 opsonization and the CR pathway for entry (a more primitive entry pathway). However, these strains demonstrate rapid *in vitro* intracellular growth. Conversely, *M. tuberculosis* strains that are heavily surface-mannosylated have become more host-adapted in part by increasing surface mannosylation with mannans that resemble the glycoforms of eukaryotic mannoproteins that are normally recycled by the homeostatic MR (4). In support of this concept, *M. tuberculosis* was recently found to contain a mammalian mannosyltransferase homologue (41), thus establishing that the process of mannosylation is conserved at least to some extent between *M. tuberculosis* and eukaryotic organisms. This concept of *M. tuberculosis* pathways mimicking aspects of human biosynthetic pathways is further supported by recent studies revealing other typical eukaryotic amino sugar substitutions on components of the *M. tuberculosis* cell envelope (42, 43).

Thus, more host-adapted *M. tuberculosis* strains expose a large and heavily mannosylated ManLAM and greater amounts of higher order PIMs that bind to the MR. Such strains are optimized in phagocytosis by cooperatively engaging the MR and CRs. Use of the mannolipoglycan/MR pathway provides a safe portal for *M. tuberculosis* within the macrophage by regulating the trafficking of bacteria and cytokine response. These strains grow more slowly in the macrophage and cause less tissue damage during infection. We speculate that such host-adapted strains would be highly successful in establishing an infection in humans but would more likely lead to the latent state rather than to an active disease state following infection. Further studies using banks of *M. tuberculosis* clinical isolates to define macrophage interactions are necessary to enhance our understanding of the molecular mechanisms of phagocytosis and *M. tuberculosis* intracellular adaptation to the human host.

Acknowledgments—We thank Drs. Joanne Turner and Charles Cottrell for assistance in flow cytometry and NMR studies, respectively. We also thank Dr. Kari Green-Church and Nan Kleinholz (Campus Chemical Instrument Center at Ohio State University) for technical support and the Central Microscopy Research Facility at the University of Iowa.

REFERENCES

1. World Health Organization (2007) *Global Tuberculosis control surveillance, planning, and financing*, World Health Organization Press, Geneva, Switzerland
2. Kang, P. B., Azad, A. K., Torrelles, J. B., Kaufman, T. M., Beharka, A., Tibesar, E., Desjardin, L. E., and Schlesinger, L. S. (2005) *J. Exp. Med.* **202,** 987–999
3. Torrelles, J. B., Azad, A. K., and Schlesinger, L. S. (2006) *J. Immunol.* **177,** 1805–1816
4. Martinez-Pomares, L., Linehan, S. A., Taylor, P. R., and Gordon, S. (2001) *Immunobiology* **204,** 527–535
5. Briken, V., Porcelli, S. A., Besra, G. S., and Kremer, L. (2004) *Mol. Microbiol.* **53,** 391–403
6. Schlesinger, L. S., Hull, S. R., and Kaufman, T. M. (1994) *J. Immunol.* **152,** 4070–4079
7. Schlesinger, L. S., Kaufman, T. M., Iyer, S., Hull, S. R., and Marciando, L. K. (1996) *J. Immunol.* **157,** 4568–4575
8. Sreevatsan, S., Pan, X., Stockbauer, K. E., Connell, N. D., Kreiswirth, B. N., Whittam, T. S., and Musser, J. M. (1997) *Proc. Natl. Acad. Sci. U. S. A.* **94,** 9869–9874
9. Manca, C., Tsenova, L., Barry, C. E., III, Bergtold, A., Freeman, S., Haslett, P. A., Musser, J. M., Freedman, V. H., and Kaplan, G. (1999) *J. Immunol.* **162,** 6740–6746
10. Manca, C., Tsenova, L., Bergtold, A., Freeman, S., Tovey, M., Musser, J. M., Barry, C. E., III, Freedman, V. H., and Kaplan, G. (2001) *Proc. Natl. Acad. Sci. U. S. A.* **98,** 5752–5757
11. Valway, S. E., Sanchez, M. P. C., Shinnick, T. F., Orme, I., Agerton, T., Hoy, D., Jones, J. S., Westmoreland, H., and Onarato, I. M. (1998) *N. Engl. J. Med.* **338,** 633–639
12. Takiff, H. E., Salazar, L., Guerrero, C., Philipp, W., Mun Huang, W., Kreiswirth, B., Cole, S. T., Jacobs, W. R., Jr., and Telenti, A. (1994) *Antimicrob. Agents Chemother.* **38,** 773–780
13. Rouse, D. A., DeVito, J. A., Li, Z. M., Byer, H., and Morris, S. L. (1996) *Mol. Microbiol.* **22,** 583–592
14. Reed, M. B., Domenech, P., Manca, C., Su, H., Barczak, A. K., Kreiswirth, B. N., Kaplan, G., and Barry, C. E., III (2004) *Nature* **431,** 84–87
15. Cox, J. S., Chen, B., McNeil, M., and Jacobs, W. R., Jr. (1999) *Nature* **402,** 79–83
16. Reed, M. B., Gagneux, S., Deriemer, K., Small, P. M., and Barry, C. E., III (2007) *J. Bacteriol.* **189,** 2583–2589
17. Sreevatsan, S., Escalante, P., Pan, X., Gillies, D. A., II, Siddiqui, S., Khalaf, C. N., Kreiswirth, B. N., Bifani, P., Adams, L. G., Ficht, T., Perumaalla, V. S., Cave, M. D., Van Embden, J. D. A., and Musser, J. M. (1996) *J. Clin. Microbiol.* **34,** 2007–2010
18. Schlesinger, L. S., Bellinger-Kawahara, C. G., Payne, N. R., and Horwitz, M. A. (1990) *J. Immunol.* **144,** 2771–2780
19. Schlesinger, L. S. (1993) *J. Immunol.* **150,** 2920–2930
20. Torrelles, J. B., Khoo, K. H., Sieling, P. A., Modlin, R. L., Zhang, N., Marques, A. M., Treumann, A., Rithner, C. D., Brennan, P. J., and Chatterjee, D. (2004) *J. Biol. Chem.* **279,** 41227–41239

21. Kaur, D., Lowary, T. L., Vissa, V. D., Crick, D. C., and Brennan, P. J. (2002) *Microbiology* **148,** 3049–3057
22. Chatterjee, D., Lowell, K., Rivoire, B., McNeil, M. R., and Brennan, P. J. (1992) *J. Biol. Chem.* **267,** 6234–6239
23. Prinzis, S., Chatterjee, D., and Brennan, P. J. (1993) *J. Gen. Microbiol.* **139,** 2649–2658
24. Berg, S., Starbuck, J., Torrelles, J. B., Vissa, V. D., Crick, D. C., Chatterjee, D., and Brennan, P. J. (2005) *J. Biol. Chem.* **280,** 5651–5663
25. Dubois, M., Gilles, K., Hamilton, J. K., Rebers, P. A., and Smith, F. (1951) *Nature* **168,** 167
26. McCarthy, T. R., Torrelles, J. B., Macfarlane, A. S., Katawczik, M., Kutzbach, B., Desjardin, L. E., Clegg, S., Goldberg, J. B., and Schlesinger, L. S. (2005) *Mol. Microbiol.* **58,** 774–790
27. Olakanmi, O., Britigan, B. E., and Schlesinger, L. S. (2000) *Infect. Immun.* **68,** 5619–5627
28. Wileman, T. E., Lennartz, M. R., and Stahl, P. D. (1986) *Proc. Natl. Acad. Sci. U. S. A.* **83,** 2501–2505
29. Nigou, J., Gilleron, M., Brando, T., Vercellone, A., and Puzo, G. (1999) *Glycoconj. J.* **16,** 257–264
30. McNeil, M. R., Robuck, K. G., Harter, M., and Brennan, P. J. (1994) *Glycobiology* **4,** 165–174
31. Chatterjee, D., Hunter, S. W., McNeil, M., and Brennan, P. J. (1992) *J. Biol. Chem.* **267,** 6228–6233
32. Chatterjee, D., Bozic, C. M., McNeil, M., and Brennan, P. J. (1991) *J. Biol. Chem.* **266,** 9652–9660
33. Delmas, C., Gilleron, M., Brando, T., Vercellone, A., Gheorghui, M., Riviere, M., and Puzo, G. (1997) *Glycobiology* **7,** 811–817
34. Venisse, A., Berjeaud, J.-M., Chaurand, P., Gilleron, M., and Puzo, G. (1993) *J. Biol. Chem.* **268,** 12401–12411
35. Turnbull, W. B., Shimizu, K. H., Chatterjee, D., Homans, S. W., and Treumann, A. (2004) *Angew. Chem Int. Ed Engl.* **43,** 3918–3922
36. Khoo, K.-H., Dell, A., Morris, H. R., Brennan, P. J., and Chatterjee, D. (1995) *Glycobiology* **5,** 117–127
37. Schlesinger, L. S., Azad, A. K., Torrelles, J. B., Roberts, E., Vergne, I., and Deretic, V. (2008) in *Handbook of Tuberculosis: Immunology and Cell Biology* (Kaufmann, S. H. E., and Britton, W. J., eds) Wiley-VCH Verlag, Weinheim, Germany
38. Chatterjee, D., and Khoo, K.-H. (1998) *Glycobiology* **8,** 113–120
39. Khoo, K.-H., Tang, J.-B., and Chatterjee, D. (2001) *J. Biol. Chem.* **276,** 3863–3871
40. Fenton, M. J., Riley, L. W., and Schlesinger, L. S. (2005) in *Tuberculosis and the Tubercle Bacillus* (Cole, S. T., Eisenach, K. D., McMurray, D. N., and Jacobs, W. R., Jr., eds) American Society for Microbiology Press, New York
41. VanderVen, B. C., Harder, J. D., Crick, D. C., and Belisle, J. T. (2005) *Science* **309,** 941–943
42. Draper, P., Khoo, K. H., Chatterjee, D., Dell, A., and Morris, H. R. (1997) *Biochem. J.* **327,** 519–525
43. Bhamidi, S., Scherman, M. S., Rithner, C. D., Prenni, J. E., Chatterjee, D., Khoo, K. H., and McNeil, M. R. (2008) *J. Biol. Chem.* **283,** 12992–13000